# Numerical validation of axial plasma momentum lost to a lateral wall induced by neutral depletion

Yoshinori Takao and Kazunori Takahashi

Citation: Physics of Plasmas **22**, 113509 (2015); doi: 10.1063/1.4935903
View online: http://dx.doi.org/10.1063/1.4935903
View Table of Contents: http://scitation.aip.org/content/aip/journal/pop/22/11?ver=pdfcov
Published by the AIP Publishing



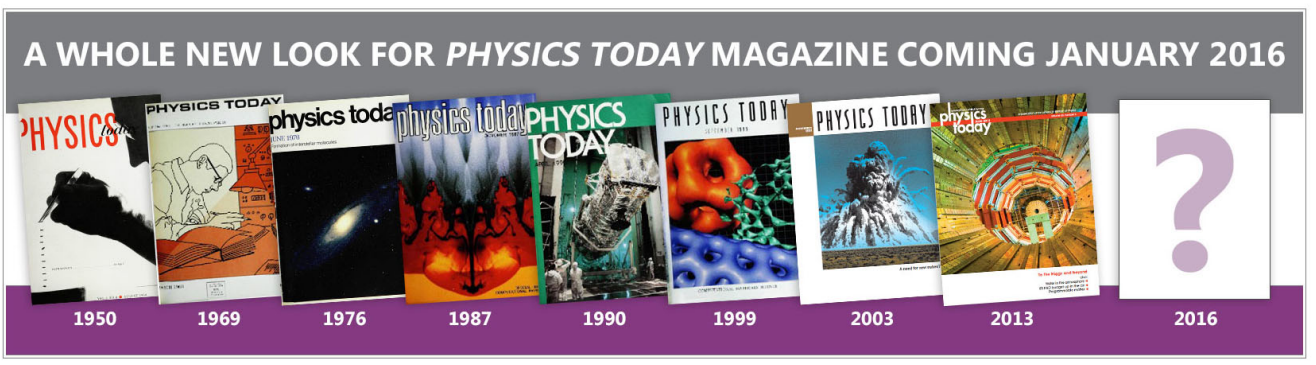

# Numerical validation of axial plasma momentum lost to a lateral wall induced by neutral depletion

Yoshinori Takao[1,a)] and Kazunori Takahashi[2]
[1]*Division of Systems Research, Yokohama National University, Yokohama 240-8501, Japan*
[2]*Department of Electrical Engineering, Tohoku University, Sendai 980-8579, Japan*

(Received 16 September 2015; accepted 3 November 2015; published online 18 November 2015)

Momentum imparted to a lateral wall of a compact inductively coupled plasma thruster is numerically investigated for argon and xenon gases by a particle-in-cell simulation with Monte Carlo collisions (PIC-MCC). Axial plasma momentum lost to a lateral wall is clearly shown when axial depletion of the neutrals is enhanced, which is in qualitative agreement with the result in a recent experiment using a helicon plasma source [Takahashi *et al.*, Phys. Rev. Lett. **114**, 195001 (2015)]. The PIC-MCC calculations demonstrate that the neutral depletion causes an axially asymmetric profile of the plasma density and potential, leading to axial ion acceleration and the non-negligible net axial force exerted to the lateral wall in the opposite direction of the thrust. © *2015 AIP Publishing LLC*. [http://dx.doi.org/10.1063/1.4935903]

## I. INTRODUCTION

Almost all steady-state plasmas in artificial devices contact with the physical wall and are sustained by balancing the electron and ion fluxes lost from the system via a sheath structure. Since plasma behavior is often modeled with momentum equations, the momentum of the charged particles is an essential parameter associated with the plasma characteristics, where momentum is conserved in both the plasma and sheath regions. In cylindrical plasma models,[1] the radial and axial momentum balances are decoupled by assuming a negligible radial variation of the axial momentum. This assumption seems to be equivalent to neglecting the axial momentum taken away from the system to the radial wall by the radially lost ions; it is also assumed to be negligible in a one-dimensional model.[2,3]

A recent experiment using a helicon plasma source detected the non-negligible axial momentum lost to the radial wall boundary for the density profile having a maximum at the upstream side of the axial center of the source.[4] This finding suggested that the ions traveling from the upstream maximum density position to an open source exit experience a longer distance with the strong density decay and are accelerated along the axis. When they are lost to the wall, axial momentum is transferred to the radial wall boundary; hence, the previously neglected term seems to affect the momentum balance equation. Furthermore, enhancement of the momentum loss process has been observed for highly ionized plasma and is considered to be induced by a neutral depletion, and the resultant axial density decay and electric field inside the source tube, where the neutrals are injected from the upstream side of the tube and various rare gas species are tested.

The aforementioned momentum loss process affects both the plasma characteristic and the performance of electric propulsion devices, since the thrust imparted by a propulsion device corresponds to the axial momentum transferred from the system into space. When the loss of the axial momentum to the radial wall occurs between the maximum density region and the thruster (source) exit, the momentum transferred from the device decreases, and the thruster performance is made poor. It is a crucial problem to clarify the momentum balance at plasma-wall interfaces.

In a recent experiment, only the net axial momentum lost to the radial wall was measured;[4] diagnosis of the local momentum is very difficult near the plasma-wall boundary. Furthermore, the measurement of the electric field in two dimensions has not been performed. Even though the plasma inside the source tube has been shown to be affected by a neutral depletion theoretically[1–3,5] and experimentally,[6,7] the depletion effect on the momentum loss to the radial source boundaries has not been discussed. Some of these models have suggested that the plasma density profile on the axis is modified due to neutral depletion effect when introducing the gas from the upstream side.[1–3] In this situation, the modification of the plasma structure is expected to affect the plasma transport and momentum transport to the radial wall, which is indeed an important issue relating to thruster modeling and performance improvement.

Here, the aforementioned axial momentum lost to the radial wall is numerically demonstrated in a compact inductively coupled plasma (ICP) source by a particle-in-cell simulation with Monte Carlo collisions (PIC-MCC). The PIC-MCC model can solve both plasma and sheath regions self-consistently; hence, the plasma dynamics near the wall boundary are also numerically solved without any preassigned conditions of particle motion or flux at the source boundaries, which is in stark contrast to fluid and theoretical approaches. Our simulation can provide the profile of the radial and axial momentum lost to the wall and electric field inside the source. Neutral depletion is artificially introduced in the calculation to investigate its effects independently; then, the results qualitatively agree with previous experiments carried out by one of the authors.[4]

a)E-mail: takao@ynu.ac.jp

 

## II. NUMERICAL MODEL

Figure 1(a) shows a schematic diagram of our model of the compact ICP source, composed of a 0.7 mm-thick cylindrical quartz tube (the lateral wall), metal plates for both axial ends of the quartz tube, and a double-turn rf loop antenna wound around the center of the tube. The inner diameter and the length are 1 cm and 3 cm, respectively, which is roughly one sixth of the dimension of the helicon plasma source employed in a recent experiment.[4] The calculation is performed for the compact ICP at this moment due to the calculation machine capability. Since we focus on the effect of neutral depletion, the external magnetic field is not included. Argon and xenon are employed as working gases to investigate the effect of the differences in the degree of ionization. The grid spacing is set at 0.1 mm at regular intervals, and cylindrical coordinates ($r$-$z$) are employed, with the origin being placed at the radial center of the left end (i.e., the upstream back plate).

The total thrust is obtained from the sum of pressure force to the source back plate $T_s$ and the force to the lateral wall in the axial direction $T_{w,z}$ in the absence of an external magnetic field. According to the theoretical models, these forces are defined as follows,[8–10] together with the force to the lateral wall in the radial direction $T_{w,r}$:

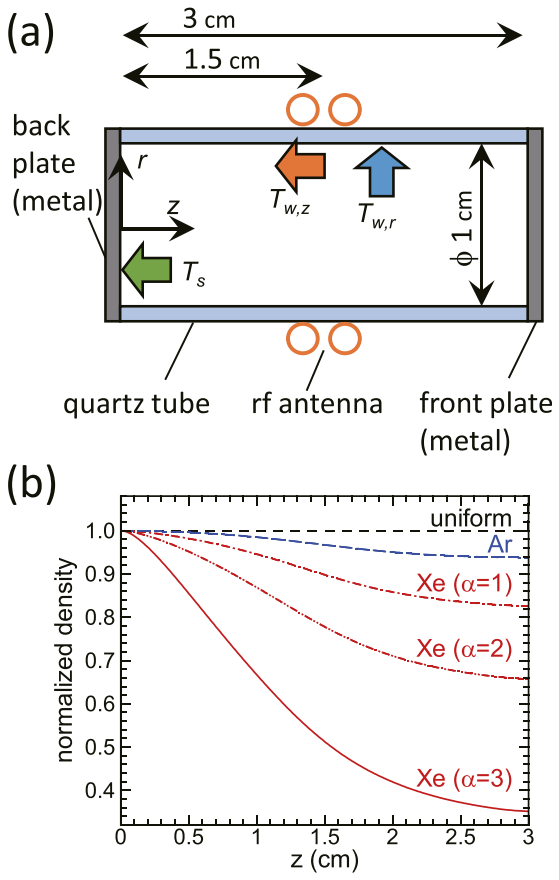


FIG. 1. (a) Schematic diagram of the simulation area for the compact ICP source, where the positive direction of each force ($T_s$, $T_{w,z}$, and $T_{w,r}$) is also defined. (b) Axial profiles of the normalized gas density for argon (blue) and xenon (red), depending on the factor of depletion α, together with the uniform profile. For argon, the factor of depletion corresponds to $\alpha = 2$.

$$T_s = 2\pi \int_0^{r_s} r p_e(r, z_0) dr, \tag{1}$$

$$T_{w,z} = -2\pi \int_0^{z_e} r_s m n(r_s, z) u_r(r_s, z) u_z(r_s, z) dz, \tag{2}$$

$$T_{w,r} = -2\pi \int_0^{z_e} r_s m n(r_s, z) u_r(r_s, z) u_r(r_s, z) dz, \tag{3}$$

where $r_s$, $z_e$, $p_e$, $z_0$, $m$, $n$, $u_r$, and $u_z$ are the radius of the lateral wall, position of the front plate (3 cm in this case), electron pressure, maximum pressure position, ion mass, density, and radial and axial ion velocities, respectively. Equations (2) and (3) imply the axial momentum $mu_z$ and the radial momentum $mu_r$ delivered by radially lost ions with the flux $nu_r$, respectively. The positive direction of each force ($T_s$, $T_{w,z}$, and $T_{w,r}$) is defined in Fig. 1(a). Although the force $T_{w,r}$ does not affect the total thrust because of its direction, the component would also be important since the radial pressure in a magnetic nozzle would be converted into the axial momentum corresponding to the thrust.[11] When neglecting the radial loss of the ions, the force exerted to the back plate in the previous fluid model corresponds to the maximum electron pressure, which is converted into the axial ion momentum by the sheath acceleration.[11] This model has already been validated in several experiments.[9,12–14] In the present simulation, the axial momentum of ions impinging on the upstream wall can be directly calculated by counting the total momentum of axially lost ions, as is the case with the momentum of ions entering the lateral wall.

The present PIC-MCC model generally follows the methodology described in our previous papers and references therein,[15–18] except that the neutral depletion is taken into consideration here, as shown in Fig. 1(b), which will be described later in this section. The PIC-MCC model consists of the electromagnetic equation for the rf-induced azimuthal electric field, the Poisson equation for the electrostatic field due to the space charge, the equation of motion, and collisions of charged particles. The assumptions in the model are as follows. (i) Only singly ionized $Xe^+/Ar^+$ and electrons are treated as particles. (ii) The reactions taken into account are elastic, excitation, and ionization collisions for electrons, and elastic and charge exchange collisions for ions. The cross-section dataset of xenon of an earlier study[18] are used, likewise for argon.[17] (iii) The motion of excited-state atoms and Coulomb collisions (electron-electron, ion-ion, and electron-ion) are not taken into account.

To couple the rf power to the plasma, the following electromagnetic equation is solved:

$$\left(\frac{\partial^2}{\partial r^2} + \frac{1}{r}\frac{\partial}{\partial r} + \varepsilon_0 \mu_0 \omega^2 - \frac{1}{r^2} + \frac{\partial^2}{\partial z^2}\right) \tilde{E}_\theta = i\omega\mu_0 \tilde{j}_\theta, \tag{4}$$

where $\varepsilon_0$, $\mu_0$, $\omega$, $\tilde{E}_\theta$, and $\tilde{j}_\theta$ are the electric permittivity of a vacuum, the magnetic permeability of a vacuum, rf angular frequency, complex amplitudes of the rf induced electric field, and the plasma current density, respectively. To derive Eq. (4), we assume that all wave quantities vary harmonically in time as $e^{i\omega t}$, where $i$ is the square root of $-1$ and $t$ is the time, and the rf antenna coil is composed of two

concentric rings. Then, $E_\theta$ and $j_\theta$ are set to be $E_\theta = \tilde{E}_\theta e^{i\omega t}$ and $j_\theta = \tilde{j}_\theta e^{i\omega t}$, respectively. The boundary conditions of $\tilde{E}_\theta$ are set to zero on both the back and front plate assuming perfectly conducting materials and on the $z$-axis ($r = 0$) owing to the axisymmetry. On the plasma-dielectric interfaces, the electric field is analytically derived from Biot-Savart's law, which is the sum of the fields over the two-turn coil current $I_{coil}$ and the plasma current.[19–22] The time-varying magnetic field ($B_r$, $B_z$) is then obtained from Faraday's law with the electric field determined by Eq. (4). The plasma current density is directly obtained by following electron trajectories, where the ion current density can be ignored owing to the low mobility. Since we focus on the results at steady state, the rf electromagnetic fields are updated every 10 rf cycles to reduce the calculation cost. The total power absorption is used as an input parameter; we rescale $I_{coil}$ to yield the specified total power absorption until the steady-state solution is obtained. The total power absorbed by the plasma is obtained by calculating the change in kinetic energy of electrons and ions before and after each charged particle is moved on integrating the equation of motion.[23]

The dielectric region is also included in the potential calculation, although the simulation area for charged particles is only the plasma region. It is assumed that a Faraday shield is inserted between the rf antenna coil and the dielectric tube, i.e., the coil is electrostatically shielded, and thus, the potential is fixed at zero over the entire dielectric region with $r = 0.57$ cm as a boundary condition: the discharge is purely inductive coupling. The boundary conditions of the potential are also zero on both back and front plate. On the plasma-dielectric interfaces, the surface charge accumulation on the dielectric is also taken into account and obtained from the summation of the charged particles incident thereon. The electric fields on the plasma-dielectric boundaries are solved using half-size Gaussian pill boxes.[24]

Initially, spatially uniform ions and electrons with Maxwellian velocities are loaded in the simulation area, where the total number of electron and ion superparticles is set at about 1 500 000. In order to speed up the simulation, ions motion and collisions are calculated only once per 25 electron time steps, owing to their difference in the speed of motion. Here, the numerical time step for electrons $\Delta t_e$ is taken to be $5.0 \times 10^{-12}$ s, which is sufficient to resolve the electron plasma frequency and is much smaller than the mean free time in every case. About $2 \times 10^6$ time steps (10 $\mu$s) are required to obtain the steady-state solution. The macroscopic parameters, such as the electron density, plasma potential, and force densities, are determined by averaging over 10 $\mu$s after steady state is reached.

To investigate the effect of neutral depletion on the thruster performance, we obtain the axial profiles of the neutral density, as shown in Fig. 1(b), using the following procedure, where the neutrals are treated as a background value at each grid point, and the neutral density is assumed to be uniform in the radial direction for simplicity. The neutral density on each grid $n_{g,i}$ is reduced based on the radially averaged degree of ionization on its left grid $a_{i-1}$, where $i$ is the grid index in the axial $z$ direction. To obtain $a_i$, we first calculate the radially averaged plasma density $n_{p,i}$ and then $a_i$ is taken from $a_i = n_{p,i}/(n_{g,i} + n_{p,i}) \simeq n_{p,i}/n_{g,i}$. Hence, the neutral density $n_{g,i}$ results from $n_{g,i} = n_{g,i-1}(1 - a_{i-1}) = n_{g,i-1} - n_{p,i-1}$. This procedure is iterated from the left end (corresponding to the gas injection in the thruster) to the right end (corresponding to the open source exit in the thruster) in the simulation area through the entire calculation time until the steady-state solution is obtained. The factor of depletion $\alpha$ is also introduced, where the degree of ionization is artificially enhanced and the neutrals are more depleted with increasing $\alpha$. Figure 1(b) shows the obtained axial profile of the neutral density for argon and xenon with various values of $\alpha$. It is found that the non-uniformity of the neutrals is enhanced by the factor $\alpha$, especially in xenon. It should be noted that the axial profile of the neutral density is dependent on the grid number in the axial direction using this procedure, and thus, the distributions of neutrals shown in Fig. 1(b) are not obtained self-consistently based on the actual degree of ionization, which is artificially controlled.

We focus on only the ion motion derived from the asymmetric distribution of the plasma; the gas dynamics of neutral particles are not taken into account, although the depleted distribution is considered. Hence, we employ a closed plasma source, as shown in Fig. 1(a), where the right end of the plasma source is also bounded by a metal wall. This boundary condition enables us to accelerate the calculation speed by using a fast Fourier transformation for solving Poisson's equation in the axial $z$ direction.[25]

In previous experiments, the pressures measured at the chamber are 1.4 mTorr for argon and 0.6 mTorr for xenon.[4] Since the size of the plasma source is reduced by one-sixth in the simulations, the neutral pressure is increased by six times to maintain the equal ratio of the mean free path to the chamber size, where the pressures of argon and xenon are 8.4 mTorr and 3.6 mTorr, respectively. The rf frequency is set at 80 MHz, which is also roughly six times 13.56 MHz in the experiment to equal the ratio of the collision frequency to the rf driven frequency. The neutral densities for argon and xenon at the left end of the tube are $2.70 \times 10^{14}\,\mathrm{cm}^{-3}$ and $1.16 \times 10^{14}\,\mathrm{cm}^{-3}$, respectively, which are obtained from the pressures of 8.4 mTorr and 3.6 mTorr with the gas temperature of 300 K.

## III. RESULTS AND DISCUSSION

The PIC-MCC simulations are conducted at the absorbed power of 1 W for each neutral distribution in Fig. 1(b). Figure 2 shows the axial profiles of the calculated force densities to the lateral wall in the axial direction ($T_{w,z}/A$) and in the radial direction ($T_{w,r}/A$), where the positive direction of each force ($T_{w,z}$ and $T_{w,r}$) is defined in Fig. 1(a) and $A$ represents the dimensions of the surface area. The negative value of the force density $T_{w,z}/A$ in Fig. 2(a) indicates that the force is imparted to the positive $z$ direction, leading to a negative effect on propulsive performance. Here, since the neutral motion is not taken into account in the PIC-MCC model and the electron mass is negligible compared to the ion mass, the forces of $T_{w,z}$ and $T_{w,r}$ are obtained by calculating only the ion momentum delivered to the lateral wall in

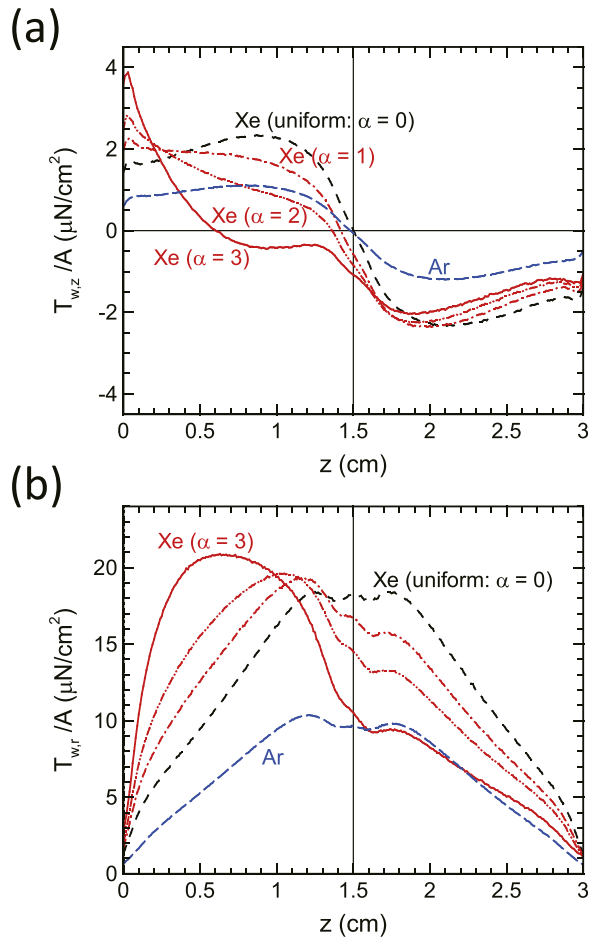


FIG. 2. Axial profiles of the calculated force densities to the lateral wall (a) in the axial direction ($T_{w,z}/A$) and (b) in the radial direction ($T_{w,r}/A$) for each profile of the neutral density, as shown in Fig. 1. Thin lines at $z = 1.5$ and $T_{w,z} = 0$ are also plotted as visual guides.

each direction. Hence, the force imparted to the wall is underestimated in the present model.

As shown in Fig. 2(a), when the neutral profile is uniform ($\alpha = 0$) for xenon, the perfectly point-symmetric profile of $T_{w,z}/A$ with respect to the axial center of the source tube is seen: the value of $T_{w,z}/A$ is zero at $z = 1.5$ cm. The force imparted to the positive $z$ direction cancels out that imparted to the negative $z$ direction, resulting in a net zero force to the lateral wall in the axial direction. However, with increasing the factor of depletion $\alpha$, the profile of $T_{w,z}/A$ becomes axially asymmetric; the axial position of $T_{w,z}/A = 0$ moves from the axial center to the back plate side of the source tube. The net force of $T_{w,z}$ integrating $T_{w,z}/A$ over the surface area of the source tube results in more negative values, demonstrating that the loss of the axial momentum to the lateral wall is enhanced by the artificially introduced factor $\alpha$, i.e., by the neutral depletion, as suggested in a recent experiment.[4] The axial asymmetry of the force density in the radial direction $T_{w,r}/A$ is also enhanced by the increase in $\alpha$. The values of $T_{w,r}/A$ are larger than those of $T_{w,z}/A$, indicating that the main momentum loss to the lateral wall is still derived from the radial momentum loss, even though the axial momentum loss cannot be neglected. For reference, $T_{w,r}/A$ and $T_{w,z}/A$ of argon plasma with $\alpha = 2$ are also plotted in Fig. 2. The axial profile of $T_{w,z}/A$ is slightly point-asymmetric with respect to the axial center, because of less neutral depletion derived from the low degree of ionization of argon compared to xenon.

Two-dimensional distributions of the electron density and potential in steady state are shown in Fig. 3 for xenon, depending on the factor of depletion $\alpha$. When the uniform neutral profile is maintained ($\alpha = 0$), the perfectly symmetric profile of electron density and potential with respect to the axial center of the source tube is obtained. Thus, the axially symmetric profile of $T_{w,z}/A$ is obtained as shown in Fig. 2(a), resulting in the net zero force to the lateral wall. As clearly seen in Figs. 3(b)–3(d), the density and potential profiles become more axially asymmetric with respect to the axial center of the source tube with increasing $\alpha$. The positions of the maximum density and potential are shifted to the more upstream side because the neutral is depleted in the downstream side. The depletion reduces the collision of ionization, resulting in a decrease in plasma density downstream of the axial center, although the peak of the azimuthal electric field induced by the rf current is still at the center of the source tube, where the rf antenna is located. In the present simulations, the absorbed power in the plasma is fixed at 1 W for all neutral density profiles. The decrease in electron density requires a higher rf antenna current to absorb the power of 1 W.[16] Such high antenna currents result in higher azimuthal electric field and an increase in number of high-energy electrons. When the neutral density is uniform, such high-energy electrons produce a higher ionization rate and then lose their energy, which results in the electron temperature being almost independent of the rf power or electric field.[17,26,27] However, when the neutral density is depleted, a higher electron temperature is obtained because of the decrease in collision of ionization. A higher electron temperature leads to a higher ionization rate, and thus maintains the ionization balance to sustain the plasma discharge. As a result, a higher peak potential is obtained with increasing the factor of depletion $\alpha$, as shown in Fig. 3.

The shift of the peak potential to the upstream side leads to the axially asymmetric profile of electric field. The ions accelerated into the positive $z$ direction by such an asymmetric electric field travel a long distance inside the source; axial momentum is delivered to the lateral wall by these ions when they are lost to the lateral wall. Although this axial momentum loss process has been proposed by the directly and individually measured negative value of $T_w$ in a previous experiment,[4] measurements of the plasma potential have not been performed. The present simulation clearly validates this loss process induced by the asymmetric density and potential profiles.

The effect of neutral depletion on the plasma power losses at each wall is also investigated, as shown in Fig. 4, where the power loss at the wall is equal to the sum of ion and electron wall losses and the rest of the power loss is composed of the sum of the power lost to ion-neutral and electron-neutral collisions.[16] The power loss at the radial wall is the major loss component, because of the largest surface area of the plasma source, and slightly increases from 380 to 412 mW with increasing $\alpha$. Although the power loss

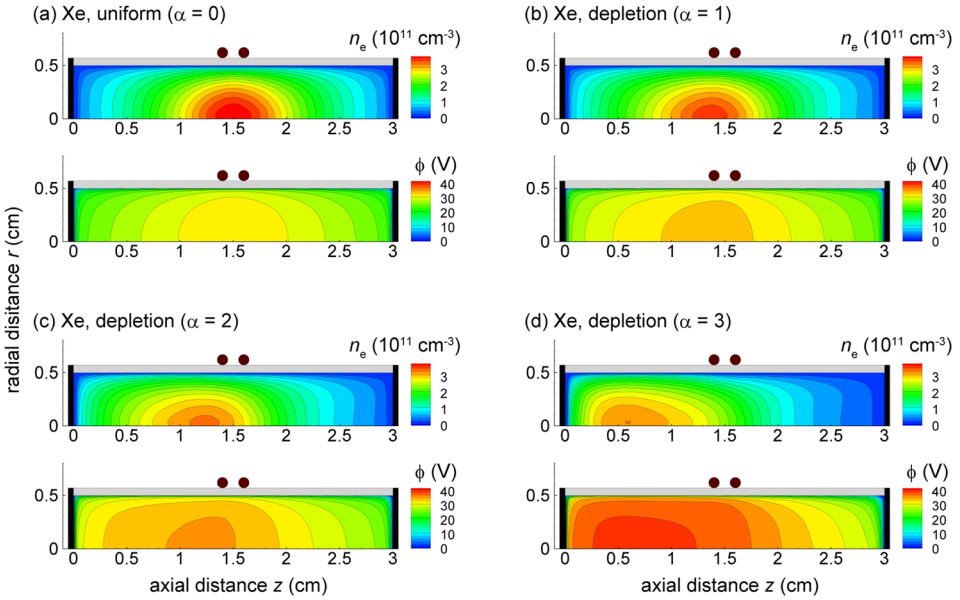


FIG. 3. Two-dimensional distributions of the time-averaged electron density and potential in steady state for each profile of the neutral density, as shown in Fig. 1 for xenon only.

at the front wall (corresponding to the thruster exit) is independent of α, the power loss at the source back wall significantly increases from 25 to 85 mW with the increasing α. This increase in power loss at the back wall is due to the shift of the peak plasma density to the upstream side. Figure 4 clearly shows that power losses on the radial and back walls are the major component of the power loss; moreover, neutral depletion enhances these losses. The result indicates that most of the power does not exit the thruster and very little rf input power goes into ion beams, which reduces the thruster performance. This tendency has also been predicted in a previous thruster model.[2]

Figure 5 shows the ratio of the net force to the lateral wall in the axial direction to that to the source back plate $T_{w,z}/T_s$ as a function of the factor of depletion α. As expected from the result of Fig. 2(a), the net force of $T_{w,z}$ is zero when the profile of the neutral density is uniform ($\alpha = 0$), and thus, the ratio $T_{w,z}/T_s$ is also zero. The increase in the factor α enhances the net force $T_{w,z}$ in the positive $z$ direction (the negative value of $T_{w,z}$) and the value of $T_{w,z}/T_s$ becomes more negative, which would degrade the thruster performance. Owing to the low degree of ionization for argon and the slight depletion of the neutral density as shown in Fig. 1(b), the negative value of $T_{w,z}/T_s$ is also small even for $\alpha = 2$. The difference in the neutral depletion effect on the momentum loss between argon and xenon is qualitatively consistent with a recently performed experiment,[4] while it should be mentioned that our simulation does not include the external magnetic field. In the case of $\alpha = 3$ for xenon, the value of $T_{w,z}/T_s$ is calculated to be about −0.33; therefore, the loss to the lateral wall cannot be neglected.

The present simulation is performed in the absence of a magnetic field for simply analyzing only the neutral depletion effects, while the helicon thruster definitely requires a magnetic field for plasma production via wave-plasma interaction and plasma expansion along a magnetic nozzle. Actually, the reduction of the radial loss of axial momentum seems to occur in the earlier experiment,[4] especially for the argon propellant case. On the other hand, momentum loss is enhanced by increasing the magnetic field strength for

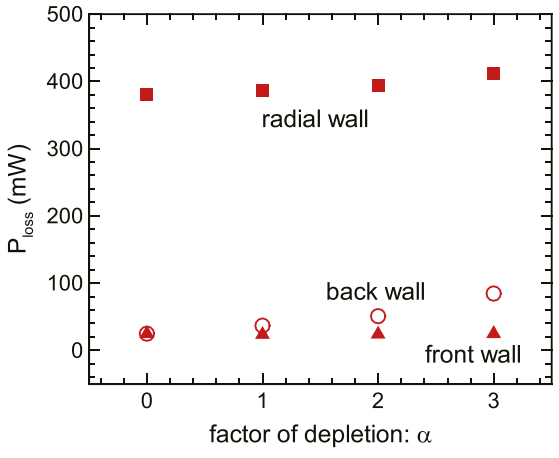


FIG. 4. Power losses $P_{loss}$ at the radial wall (square), back plate (circle), and front wall (delta) as a function of the factor of depletion α for each profile of the neutral density, as shown in Fig. 1 for xenon only.

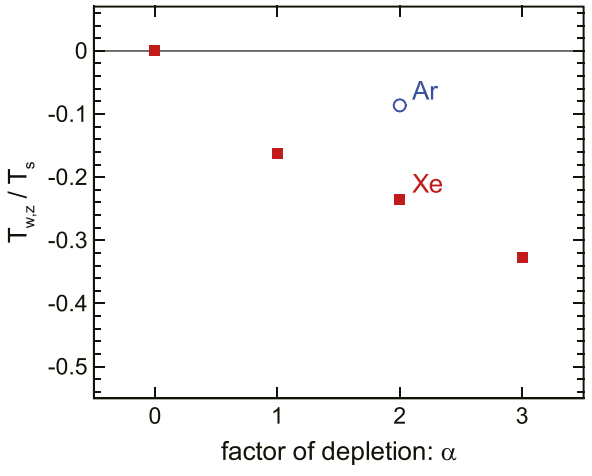


FIG. 5. Ratio of the force to the lateral wall in the axial direction to that to the source back plate $T_{w,z}/T_s$ as a function of the factor of depletion α for each profile of the neutral density, as shown in Fig. 1.

krypton and xenon cases. These different tendencies seem to compete between the inhibition effect by the magnetic field and the enhancement by the neutral depletion.[4] Since the different effects seem to be nonlinearly coupled in the experiment, our simulation plays an important role in investigating these effects independently. The introduction of an external magnetic field will be progressed hereafter.

It should be noted that the potential structure derived from the Boltzmann relation is a function of the plasma density ratio, not the plasma density itself. Even though the plasma density of argon is lower than that of xenon, the axial momentum loss of argon could be more significant than that of xenon if the density profile of argon is more axially asymmetric than that of xenon. Actually, the relatively large negative value of $T_w$ was obtained for argon without an applied magnetic field in the previous experiment because of the axially asymmetric density profile.[12] The neutral density profile is usually not taken into account and is often treated as uniform for numerical simulations, because its effect on the plasma characteristics and thruster performance is considered to be less significant compared to the plasma itself. However, the recent experimental[4] and the present numerical simulation results imply that the neutral depletion effect should be carefully taken into account in thruster models in the case of high power, where highly ionized plasma discharges occur as predicted by the analytical model.[3]

## IV. CONCLUSIONS

In summary, the PIC-MCC calculations are performed to validate the recently proposed momentum loss mechanism to the radial wall, where axial momentum is taken away from the plasma flow by the radially lost ions.[4] The present PIC-MCC model can solve both the plasma and sheath regions self-consistently; thus, the momentum loss at the wall is also obtained without any pre-assigned boundary conditions of particles motion or flux. The calculation demonstrates that the asymmetric density and the resultant potential profiles induce enhancement of the loss of axial momentum to the lateral wall, where the measurement of the plasma parameters near the wall boundary is difficult in experiments. It has been clearly identified that the loss process is enhanced by the neutral depletion effect, which is artificially controlled in the calculation.

## ACKNOWLEDGMENTS

This work was partially supported by grant-in-aid for scientific research (Grant No. B 25287150) from the Japan Society for the Promotion of Science and the Yazaki Memorial Foundation for Science and Technology. Part of the computer simulations was performed on the KDK computer system at the Research Institute for Sustainable Humanosphere, Kyoto University.

[1]E. Ahedo and J. Navarro-Cavallé, Phys. Plasmas **20**, 043512 (2013).
[2]T. Lafleur, Phys. Plasmas **21**, 043507 (2014).
[3]A. Fruchtman, IEEE Trans. Plasma Sci. **36**, 403 (2008).
[4]K. Takahashi, A. Chiba, A. Komuro, and A. Ando, Phys. Rev. Lett. **114**, 195001 (2015).
[5]A. Fruchtman, G. Makrinich, P. Chabert, and J. M. Rax, Phys. Rev. Lett. **95**, 115002 (2005).
[6]R. M. Magee, M. E. Galante, J. C. G. Lusk, Jr., D. W. McCarren, and E. E. Scime, Phys. Plasmas **20**, 123511 (2013).
[7]S. Yun, K. Taylor, and G. R. Tynan, Phys. Plasmas **7**, 3448 (2000).
[8]A. Fruchtman, K. Takahashi, C. Charles, and R. W. Boswell, Phys. Plasmas **19**, 033507 (2012).
[9]K. Takahashi, T. Lafleur, C. Charles, P. Alexander, and R. W. Boswell, Phys. Rev. Lett. **107**, 235001 (2011).
[10]A. Fruchtman, Phys. Rev. Lett. **96**, 065002 (2006).
[11]K. Takahashi, T. Lafleur, C. Charles, P. Alexander, and R. W. Boswell, Phys. Plasmas **19**, 083509 (2012).
[12]K. Takahashi, C. Charles, and R. W. Boswell, Phys. Rev. Lett. **110**, 195003 (2013).
[13]K. Takahashi, T. Lafleur, C. Charles, P. Alexander, R. W. Boswell, M. Perren, R. Laine, S. Pottinger, V. Lappas, T. Harle, and D. Lamprou, Appl. Phys. Lett. **98**, 141503 (2011).
[14]T. Lafleur, K. Takahashi, C. Charles, and R. W. Boswell, Phys. Plasmas **18**, 080701 (2011).
[15]Y. Takao, M. Sakamoto, K. Eriguchi, and K. Ono, Trans. JSASS Aerosp. Technol. Jpn. **12**, Pb_13 (2014).
[16]Y. Takao, K. Eriguchi, and K. Ono, J. Appl. Phys. **112**, 093306 (2012).
[17]Y. Takao, N. Kusaba, K. Eriguchi, and K. Ono, J. Appl. Phys. **108**, 093309 (2010).
[18]Y. Takao, H. Koizumi, K. Komurasaki, K. Eriguchi, and K. Ono, Plasma Sources Sci. Technol. **23**, 064004 (2014).
[19]H. Fukumoto, I. Fujikake, Y. Takao, K. Eriguchi, and K. Ono, Plasma Sources Sci. Technol. **18**, 045027 (2009).
[20]B. W. Yu and S. L. Girshick, J. Appl. Phys. **69**, 656 (1991).
[21]X. Chen and E. Pfender, Plasma Chem. Plasma Process. **11**, 103 (1991).
[22]P. Silvester, *Modern Electromagnetic Fields* (Prentice-Hall, Englewood Cliffs, 1968), p. 153.
[23]M. Surendra and D. B. Graves, IEEE Trans. Plasma Sci. **19**, 144 (1991).
[24]V. Vahedi and G. DiPeso, J. Comput. Phys. **131**, 149 (1997).
[25]H. Takekida and K. Nanbu, IEEE Trans. Plasma Sci. **34**, 973 (2006).
[26]S. K. Nam and D. J. Economou, J. Appl. Phys. **95**, 2272 (2004).
[27]J. Hopwood, O. Minayeva, and Y. Yin, J. Vac. Sci. Technol. B **18**, 2446 (2000).